Journal of Power Sources 243 (2013) 409–418

Contents lists available at SciVerse ScienceDirect

Journal of Power Sources

journal homepage: www.elsevier.com/locate/jpowsour

Modelling of electrolyte degradation and cycling behaviour in a lithium–air battery

Ukrit Sahapatsombut*, Hua Cheng, Keith Scott

School of Chemical Engineering and Advanced Materials, Newcastle University, Merz Court, Newcastle upon Tyne NE1 7RU, UK

HIGHLIGHTS

- An electrolyte degradation model is developed for a rechargeable Li–air battery.
- The discharge products of Li_2O_2 and Li_2CO_3 are included during battery cycling.
- The model predicts the cycling behaviour and cycle life performance of battery.
- The discharge termination came from the repeated depositing of discharge products.

ARTICLE INFO

Article history:
Received 16 March 2013
Received in revised form
28 May 2013
Accepted 3 June 2013
Available online 14 June 2013

Keywords:
Li–air battery
Macro-homogeneous model
Porous cathode
Discharge products
Electrolyte degradation
Cycling behaviour

ABSTRACT

To understand the deterioration of cycle performance and energy efficiency related with non-aqueous rechargeable Li–air batteries, a micro–macro homogeneous model has been developed to include the practical feature of Li_2CO_3 formation which occurs by electrolyte degradation during battery cycling. The discharge products can limit the cyclability and passivate the porous-cathode surface. A modelling study of cycling behaviour and cell performance for Li–air batteries in a non-aqueous electrolyte is presented which includes the influence of electrolyte solution degradation. The cycle performance deterioration measured in term of retention of discharge capacity on cycling was predicted from the developed model which includes the effect of irreversible Li_2CO_3 discharge product. A good agreement between this cell cycling simulation and porous-electrode experiment data is obtained, thus creating a more reliable model for a rechargeable Li–air battery in non-aqueous electrolyte. The cell cycling simulation and porous-electrode experiment indicate that there has been gradual decrease for retention of discharge capacity in a number of battery cycles due to the effect of irreversible formation of the Li_2CO_3 discharge product. The termination of the cell discharge is not from the pore blockage by the repeated depositing of discharge products as there are some available pores at the end of each discharge cycle.

© 2013 Elsevier B.V. All rights reserved.

1. Introduction

The recent growing interest in electric vehicles (EVs) or hybrid electric vehicles (HEVs) for transportation has many merits that can contribute towards sustainable development. It is well known that the success of EVs and HEVs hinges upon energy storage devices which have high performance and low weight. The rechargeable Lithium–air (Li–air) or Lithium–oxygen (Li–O_2) batteries which match an important candidate for energy storage above have attracted much attention in recent years because of their theoretical specific energy of 1.1 × 10^4 Wh kg^{-1} by weight of lithium metal alone or about 5.2 × 10^3 Wh kg^{-1} when the oxygen weight is included [1,2]. It is estimated that practical Li–air batteries can deliver a specific energy more than 800 Wh kg^{-1}, which outperform that achievable by conventional lithium ion batteries (between 200 and 250 Wh kg^{-1}) generally applied in commercial EVs and HEVs market. Since the Li–air system with a non-aqueous electrolyte was first presented by Abraham and Jiang in 1996 [3], many aspects of development with a non-aqueous or organic electrolyte have been investigated [4–9]. Moreover, Li–air batteries have much more attention especially after their promise of rechargeable ability was demonstrated Bruce et al. [5].

A typical cell design for a Li–air battery contains a metal lithium anode, a solid separator polymer, and a porous carbon or catalyst-loaded carbon air electrode filled with an organic electrolyte comprising a dissolve lithium salt in an aprotic solvent. The advantages in using a non-aqueous system are to avoid the problem of H_2 evolution due to the reaction of lithium with water and

* Corresponding author. Tel.: +44 191 222 5207; fax: +44 191 222 5292.
E-mail address: ukrit.sahapatsombut@ncl.ac.uk (U. Sahapatsombut).

0378-7753/$ – see front matter © 2013 Elsevier B.V. All rights reserved.
http://dx.doi.org/10.1016/j.jpowsour.2013.06.043

prevent the lithium metal corrosion [10]. For the non-aqueous system, the main overall reactions during discharge process for Li–air cell are the formation of lithium peroxide (Li_2O_2) and lithium oxide (Li_2O) by the reduction reaction of O_2 with lithium ions formed from oxidation of the metallic lithium according to following reactions:

$$2Li^+ + O_2 + 2e^- \rightarrow (Li_2O_2)_{solid} \quad (E_{rev} = 2.96\ V\ vs\ Li) \qquad (I)$$

$$4Li^+ + O_2 + 4e^- \rightarrow 2(Li_2O)_{solid} \quad (E_{rev} = 2.91\ V\ vs\ Li) \qquad (II)$$

with reversible potential, E_{rev}, referenced to Li/Li^+. Although other publication reported E_{rev} for Li_2O_2 as about 3.1 V without references to the thermodynamic data [3,11], the potential values were derived from published Gibbs free energy database [12,13]. Previous studies have identified Li_2O_2 as the main reaction product in the pores of cathode after discharge, with the process being reversible on charge [1,3,5,9,14]. Up to now, there have been various proposed different mechanisms for oxygen reduction reaction (ORR) with Li^+ electrolytes depending on the type of electrolyte, catalyst and battery operating conditions. A recent in-situ spectroscopic study of oxygen reaction in non-aqueous electrolyte by Peng et al. [15] reported strong evidence that lithium superoxide (LiO_2) is indeed an intermediate species during oxygen reduction before disproportion to the final Li_2O_2 product. On charge the latter is directly oxidised into O_2 and Li^+ without going through the intermediate LiO_2 route. However, the reversibility of Li–air batteries is still far for being ideal for use as an energy storage because of the formation of many non-desired products in porous cathode. It has been demonstrated that these different discharge products strongly depend on the kinetic of the oxygen reduction, which is affected by the presence of a catalyst as well [13,14,16], and also by the type of electrolytes and solvents used in the Li–air cell [7,17–21]. Generally, the electrolytes frequently used in these Li–air batteries are based on organic carbonate-based esters as solvent owing to their success in Li-ion batteries.

Organic carbonate-based electrolytes (e.g., $LiPF_6$ in propylene carbonate, (PC) or ethylene carbonate (EC)) have been widely used in Li–air batteries [5,8,9,14,18,22,23]. However, recently it has been demonstrated that the cycle life of Li–air battery using carbonated-based electrolyte is mainly limited by the electrolyte decomposition between oxygen and electrolyte forming irreversible organic and inorganic carbonate species (i.e. lithium alkylcarbonates and Li_2CO_3) during discharge, rather than the desired Li_2O_2 which can reversible produce O_2 on charging [18,21,24–27]. Different characterization techniques have supported identification of these discharge byproducts formed by reduction of carbonate-based solvent molecules that react with superoxide radical anions ($O_2^{\cdot -}$) generated from single-electron reduction of oxygen [18,20]. Therefore, a more stable electrolyte that does not produce the irreversible byproduct formation during the cell operation is required for a truly reversible Li–air battery.

Ether-based electrolytes are now attractive for the Li–air battery because of its compatibility with lithium anode, more stable to oxidation potentials than organic carbonate solvent, safe and low volatility in case of high molecular weight [17,20]. Bruce and co-workers investigated the ether-based Li–air battery and demonstrated that the Li_2O_2 formed on first discharge and disappeared after 5 cycles [17]. However, they also found that even ethers electrolyte also decompose to give a mixture of Li_2CO_3, lithium formate (HCO_2Li), lithium acetate (CH_3CO_2Li), CO_2 and H_2O, and these discharge byproducts accumulate with further battery cycling. The stability test on the discharge products in Li–O_2 battery using the different types of organic solvents (e.g. glyme-based ether, carbonates, sulfoxides, phosphates, nitriles and ionic liquid) has been reported by Xu et al. [20]. By using various analysed techniques, a large amount of Li_2O_2 was found in the air electrode discharge in glyme-based electrolytes; however Li_2CO_3 was also clearly detected in all the electrodes during discharge from all electrolytes studied with different solvents. Moreover, a recent study by the same group [27] demonstrated that the formation of Li_2CO_3 on the active electrode surface cannot be reversed during the charging step up to 4.5 V which is higher than the reported charging voltage for Li–air battery. Therefore, Li_2CO_3 may be formed inside the porous cathode, regardless of most solvents used to date, and deteriorate the battery efficiency and short cycle life (i.e. Li–air battery cannot fully rechargeable for long cyclability).

We have provided in our previous study a model of the cycling behaviour of Li–air batteries [28], which did not take into account electrolyte degradation behaviour. In this paper a modified version for the Li–air model will include the parasitic reactions, considering the irreversible Li_2CO_3 as the main byproduct. The model predicts the time dependence of electrolyte concentration, non-uniform porosity and reaction rate. Although other byproducts besides Li_2CO_3 are formed during electrolyte decomposition, their quantities may be considered as insignificant relative to the Li_2CO_3. During discharging, the desired Li_2O_2 and irreversible Li_2CO_3 form and coexist on the active surface of carbon electrode. The results from gases analysis by mass spectrometry showed that CO_2, which could be considered as the active material to cause the Li_2CO_3 formation, are generated on discharge for both carbonate and ether based solvents, as described by Bruce group [17,18]. This model can be used to describe the behaviour of Li–air batteries as well as to optimise the performance and structure of these battery electrodes.

2. Theoretical mechanism analysis

The Li–air battery, shown in Fig. 1, contains a metallic lithium anode, a separator containing electrolyte, and a porous carbon or catalyst-loaded carbon air electrode filled with an organic electrolyte comprising a dissolve lithium salt in an aprotic solvent. During discharge, the oxidation reaction of lithium metal occurs at the lithium–electrolyte interface as follow:

$$Li(metal) \rightarrow Li^+ + e^- \quad \left(E_{ref} = 0\ V\right) \qquad (III)$$

The lithium ions (Li^+) transport through the separator to the porous cathode. The produced electrons are conducted through the external circuit towards the active cathode, where the charge transfer reduction reaction takes place with the combination of Li^+ and oxygen to form lithium oxides or Li-based compounds depending on the types of electrolyte used and the electrochemical reaction occurred in the Li–air system. As mentioned earlier, the battery electrolytes play an important role in defining whether the cathode can provide the desired electrochemical products. However, to simplify our model simulation, Li_2O_2 is the main discharged product depositing inside the porous of Li–air battery following Eq. (I) when using several non-aqueous electrolytes, e.g. organic carbonate-based or ether-based solvent. Moreover, the irreversible Li_2CO_3 formation is also considered as the main byproduct coexisting with Li_2O_2.

The exact detail of the reaction routes at the cathode can be complicated regarding several intermediates. It has been identified that the nucleophilic attack of superoxide on the O-alkyl carbon is a usual starting mechanism for decomposition of organic carbonates, alkyl carboxylates, and alkyl esters of moderately strong inorganic acids [29]. Hence, it is possible to propose a mechanism to describe the formation reaction of Li_2CO_3 can be divided into two reaction mechanisms: (1) Li_2CO_3 formation from the reaction of superoxide

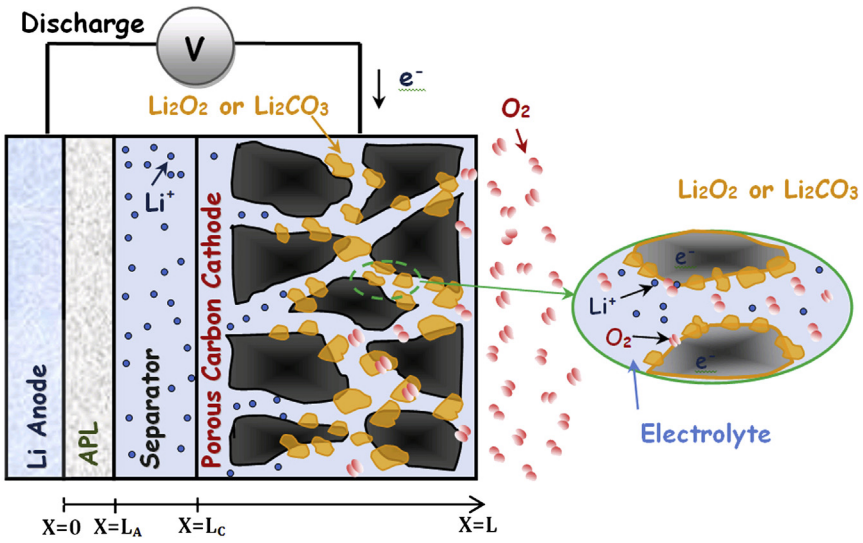

Fig. 1. Schematic computation domain of a Li–air battery during discharge operation. The inset demonstrates the discharge products formation of Li_2O_2 and Li_2CO_3 covering on the porous carbon surface.

reacts with carbon dioxide in mechanism 1 as described previously [17,30,31]; (2) the Li_2CO_3 occurs from the electrochemical reduction of CO_2, due to the electrolyte degradation with CO_2 as shown in mechanism 2, which was similar to the proposed salts formation in the solid electrolyte interface (SEI) film in Li-ion batteries [32,33].

Mechanism 1:

$$2O_2 + 2e^- \overset{k1a}{\rightarrow} 2O_2^- \quad E^0 = 3.18 \tag{1a}$$

$$2O_2^- + 2CO_2 \overset{k1b}{\rightarrow} C_2O_6^{2-} + O_2 \quad \text{RDS} \tag{1b}$$

$$C_2O_6^{2-} + 4Li^+ + 2O_2^- \rightarrow 2Li_2CO_3 + 2O_2 \tag{1c}$$

$$\text{Overall} \quad 4Li^+ + 2CO_2 + 2O_2^- + 2e^- \rightarrow 2Li_2CO_3 + O_2 \quad E^0 = 7.19 \tag{IV}$$

Mechanism 2:

$$CO_2 + e^- \overset{k2a}{\rightarrow} CO_2^- \tag{2a}$$

$$CO_2^- + CO_2 + e^- \overset{k2b}{\rightarrow} CO + CO_3^{2-} \quad \text{RDS} \tag{2b}$$

$$2Li^+ + CO_3^{2-} \rightarrow Li_2CO_3 \tag{2c}$$

$$\text{Overall} \quad 2Li^+ + 2CO_2 + 2e^- \rightarrow Li_2CO_3 + CO \quad E^0 = 2.49 \tag{V}$$

Solvent degradation:

$$O_2 + e^- \overset{k1a}{\rightarrow} O_2^- \quad E^0 = 3.18 \tag{3a}$$

$$O_2^- + [\text{Solvent}] \rightarrow [\text{Solvent}]^- \tag{3b}$$

$$[\text{Solvent}]^- + O_2 \rightarrow CO_2 + H_2O + HCO_2Li + CH_3CO_2Li \tag{3c}$$

$$\text{Overall} \quad 2O_2 + [\text{Solvent}] + e^- \rightarrow CO_2 + H_2O + HCO_2Li + CH_3CO_2Li \tag{VI}$$

Mechanism 1 commences with oxygen reduction in the porous cathode to form O_2^- in reaction (1a) which can either react with CO_2 (produced from the solvent degradation with O_2 described below) to generate the peroxydicarbonate anion $C_2O_6^{2-}$ and then Li_2CO_3 [reaction (1b) and (1c)] or may react directly with solvent in both carbonate and ether based electrolyte, in turn, leading to the intermediate species of peroxoradical and the ether peroxide, respectively [17,18]. These intermediate species can readily undergo, in the presence O_2, oxidative decomposition reactions [reaction (3c)], which are analogous to combustion reactions, leading to the formation of H_2O and CO_2 [34–36]. The oxidative decomposition also produces lithium formate and lithium acetate products which are not considered here in the model.

Mechanism 2 deals with the reduction of CO_2 in non-aqueous solvents which has been extensively studied, because CO_2 has a greater solubility in non-aqueous media than in water and is used as material feed to produce more valuable organic compounds [37]. The CO_2 reactant in this mechanism is also generated from the electrolyte degradation described above. There are many mechanism routes for reduction of CO_2 depending on cathode metals and solvents used [37]. However, one of the main reaction products are CO_3^{2-} and CO as described in reaction (2b) which can be created from the reduction of CO_2^- intermediate species (reaction (1b)) [33,37]. Hence, in the presence of Li^+ ions, the $LiCO_3$ could be formed following the route in mechanism 2 which will be consider in the model.

With the use of organic solvent for electrolyte, both Li_2O_2 and Li_2CO_3 can be produced as discharged products and are usually insoluble in the cell electrolyte. As a result, the repeated depositing film of different lithium salts over the carbon surface after each discharge and charge step prevents species transport and the electrochemical reaction, and diminishes the electronic conductivity of the air electrode and electrolyte concentration leading to cell voltage loss [25].

3. Battery model

3.1. Model description and assumptions

This work develops a one-dimensional model for a prismatic single cell of a Li–air battery which consists of a thin lithium sheet negative electrode, an anode protective layer (APL), a separator, and a porous carbon oxygen/air cathode filled with an organic electrolyte as shown in Fig. 1. Current collectors are placed at the back of each electrode. The electrolytic solution is considered as a concentrated binary electrolyte to describe the motion for of each species in the systems. For the Li–air simulation, we are particularly interested in analysing the effect of different parameters on the porous cathode, because its thickness is much larger than both of APL and separator and this area is regard as the main contribution to the cell performance. The formation of solid products inside the porous cathode is based on a macro-homogeneous porous model defining the electrode by its porosity which is initially uniform but which changes as discharge occurs.

As the Li–air battery system is complex with the various mass transport species along the cell, the build-up of Li_2O_2 and Li_2CO_3, and the change of porosity and interfacial surface area vary with time and space, several model assumptions were adopted to facilitate the calculation as follow:

- The Li–air cell is operated in isothermal conditions so that the thermal effects are not considered
- The lithium salts of Li_2O_2 and Li_2CO_3 are the main discharge products which only occur and deposit inside the porous cathode.
- The electrolytes used in Li–air batteries are assumed a binary monovalent electrolyte which consists of a single salt in a homogeneous organic solvent mixture.
- The electrolyte behaviour is based on concentrated solution theory to simulate the Li^+ diffusion.
- The pores in the cathode are full of liquid phase electrolyte such as a solution of lithium hexafluorophosphate ($LiPF_6$) in a non-aqueous solvent.
- The oxygen is assumed to dissolve in the organic electrolyte with a saturated initial concentration.
- Convective for mass transport is negligible inside the cell.

3.2. Governing equations

This section provides the governing equations which describe conservation of mass and current, species transport, and reaction kinetic in the porous cathode and separator to clarify the mechanism inside the Li–air cell mentioned above.

3.2.1. Transport of species

As the model is based on the macroscopic theory of porous electrode which considers the solution and solid matrix phases as superimposed continuum [38,39]. Based on this approach, a material balance equation for specie i transport in the Li–air electrolyte can be expressed as

$$\frac{\partial(\varepsilon c_i)}{\partial t} = -\nabla\cdot\boldsymbol{N_i} + r_i \tag{1}$$

where c_i is the bulk concentration of species i in the solution phase which is averaged over the volume of the solution in the pores, ε is the porosity of the electrode which is the electrolyte space in the solution phase, $\boldsymbol{N_i}$ is the molar flux of species i in the porous solution averaged over the cross sectional area of the electrode, and r_i is the volumetric production rate of species i from the solid phase (electrode material) to solution phase (electrolyte in the porous) within the porous electrode.

The concentration of lithium salt electrolyte is the same as concentration of Li^+ due to the binary electrolyte assumption. Without convection, the diffusion and migration fluxes equations for mass transfer of Li^+ and all of the species transporting in the porous cathode can be expressed as

$$\boldsymbol{N_{Li}} = -D_{\mathrm{Li,eff}}\nabla c_{\mathrm{Li}} + \frac{i_2 t_+}{F} \tag{2}$$

$$\boldsymbol{N_i} = -D_{i,\mathrm{eff}}\nabla c_i \tag{3}$$

where $D_{\mathrm{Li,eff}}$ and $D_{i,\mathrm{eff}}$ are the effective diffusion coefficient of Li^+ and species i, respectively, t_+ is the transference number of Li^+, F is Faraday's constant which is equal to 96,485 C mol^{-1}, and i_2 is the current density in the solution phase or electrolyte current density which can be defined by the gradient of the potential in a 1:1 binary concentrated electrolyte solution as [38,40]

$$\boldsymbol{i}_2 = -\kappa_{\mathrm{eff}}\nabla\phi_2 - \frac{2RT\kappa_{\mathrm{eff}}}{F}(t_+ - 1)\left(1 + \frac{\partial \ln f}{\partial \ln c_{\mathrm{Li}}}\right)\nabla \ln c_{\mathrm{Li}} \tag{4}$$

where κ_{eff} is the effective conductivity of the electrolyte, ϕ_2 is the electrolyte potential (electric potential of Li^+), R is the universal gas constant which is equal to 8.3143 J mol^{-1} K^{-1}, T is the cell temperature in Kelvin, and f is the activity coefficient of $LiPF_6$ salt.

In the solid matrix phase, the movement of electron is governed by Ohm's law which evaluates the electric potential variation or potential of electron, ϕ_1, as follow

$$\boldsymbol{i}_1 = -\sigma_{\mathrm{eff}}\nabla\phi_1 \tag{5}$$

where σ_{eff} is the effective conductivity of the electron in the electrode. This parameter is affected by the volume fraction of solid electrode inside the porous cathode.

Moreover, the effective parameters of $D_{i,\mathrm{eff}}$, κ_{eff} and σ_{eff} in the above equations also depend on the tortuosity of individual phases in the porous cathode (through porosity or volume fraction). These parameters are applied for only the porous cathode region and are corrected to account for the porosity effect using the Bruggeman correlation [41]

$$D_{\mathrm{Li,eff}} = \varepsilon^{1.5} D_{\mathrm{Li}} \tag{6}$$

$$D_{i,\mathrm{eff}} = \varepsilon^{1.5} D_i \tag{7}$$

$$\kappa_{\mathrm{eff}} = \varepsilon^{1.5}\kappa \tag{8}$$

$$\sigma_{\mathrm{eff}} = (1-\varepsilon)^{1.5}\sigma \tag{9}$$

where D_{Li}, D_i, κ and σ are the diffusion coefficient of the Li^+ and each specie in electrolyte and the conductivity of electrolyte and electron in the cathode, respectively.

3.2.2. Conservation of charge

For the porous electrode theory, the charge conservation for the matrix and solution phases would require the divergence of the total current density to be zero defined by

$$\nabla\cdot\boldsymbol{i}_1 + \nabla\cdot\boldsymbol{i}_2 = 0 \tag{10}$$

During discharge or charge, the electrochemical reactions occurring at the electrode/electrolyte interface (charges transfer

reaction) are expressed for individual reactions according to the conventionally general formula of the form

$$\sum s_i M_i^{z_i} \rightarrow ne^- \tag{11}$$

The charge transfer from solid phase to electrolyte phase per unit volume of electrode ($\nabla . \boldsymbol{i}_2$) is related to the individual average transfer current density occurred at the cathode given by

$$(\nabla \cdot \boldsymbol{i}_2) = \sum_m a j_m \tag{12}$$

This equation states that the transfer current per unit electrode volume is equivalent to the electrode chemical reaction rate where the M_i is a species symbol participating in the electrochemical reaction, z_i and s_i are the charge number and the stoichiometric coefficient of the species i, n is the number of electron transferred in the reaction, a is the specific interfacial area of the pore per unit volume of the total electrode, and j_m is local transfer current density between electrode and electrolyte interface of each reaction at the cathode. The value of s_i, z_i, and n can be defined by matching with an individual electrode reaction using the general form of Eq. (11), for example, the value of s_{Li}, z_{Li}, and n of Li^+ from Eq. (I) are −2, 1, and 2, respectively.

In practical Li–air cell, the precise reaction routes can be complicated regarding several intermediates as proposed in the previous reports [17,18]. Hence, both electrochemical reactions of Li_2O_2 and Li_2CO_3 formation inside porous electrode are considered in the present work. The superficial production rate of each species (referred to Eq. (1)) from solid phase to pore solution in the individual reactions m is given by Faraday's law

$$r_i = -\sum_m \frac{a s_{im}}{nF} j_m \tag{13}$$

3.2.3. Rate expressions at cathode

The actual reaction paths and mechanisms for the discharge products are not available and quite complex involving various intermediates. Hence to describe the electrochemical kinetic expression for the porous cathode the model adopts the kinetic expression based on Eq. (I) for Li_2O_2 formation and on Eqs. (IV) and (V) for Li_2CO_3 formation.

3.2.3.1. Li_2O_2 formation. For electrochemical reaction of Li_2O_2 at the cathode, a modified version of the Butler–Volmer equation is applied in the model using two rate coefficients. The reaction for Li_2O_2 formation presented in Eq. (I) also depends on the concentration of Li^+ and oxygen for discharge and the concentration of Li_2O_2 during charge as in the following equation

$$\frac{j_I}{2F} = k_a\left(c_{Li_2O_2}\right)\exp\left[\frac{(1-\beta)nF}{RT}\eta_m\right] - k_c\left(c_{Li^+}\right)^2\left(c_{O_2}\right)\exp\left[\frac{-\beta nF}{RT}\eta_m\right] \tag{14}$$

$$\eta_m = \phi_1 - \phi_2 - \Delta\phi_{film} - E_m^0 \tag{15}$$

$$\Delta\phi_{film} = j_c R_{film} \varepsilon_s \tag{16}$$

where k_a and k_c are the anodic and cathodic rate constant, respectively, β is the symmetry factor equal to 0.5, η_m is surface or activated overpotential for individual reaction, m, at the cathode, $\Delta\phi_{film}$ and R_{film} are the voltage drop and the electrical resistivity across Li_2O_2 film formation, respectively, ε_s is the volume fraction of solid formation of discharge products of Li_2O_2 and Li_2CO_3, and E_m^0 is the theoretical open-circuit potential for each reaction.

3.2.3.2. Li_2CO_3 formation. As explained before, the Li_2CO_3 formation is one of the discharge by-products coexisting with Li_2O_2. Thus, the decomposition of electrolyte, which initially forms CO_2 and finally generates Li_2CO_3 as described above, occurs during Li–air operation. Some of the elementary steps in the electrolyte degradation sequences that lead to these by-products may be irreversible and non-electrochemical, so that the overall kinetic expression is very complex. Therefore, we use the kinetics for Li_2CO_3 formation of both mechanism 1 and 2 above based on the published kinetic data.

For the mechanism 1, the superoxide radical anion that is initially formed (Eq. (1a)) during Li–air discharge as evidenced in previous study [15], attacks CO_2 which is generated from solvent decomposition (from Eq. VI) to finally form Li_2CO_3 with the presence of Li^+ as follow reaction

$$j_{1a} = Fk_{1a}\left(c_{O_2}\right)\left[-\exp\left(\frac{-\beta nF}{RT}\eta_m\right)\right] \tag{17}$$

$$r_{1b} = k_{1b}\left(c_{O_2^-}\right)\left(c_{CO_2}\right) \tag{18}$$

where k_{1a} and k_{1b} are the rate constant for the electrochemical reaction to form O_2^- and chemical reaction to generate Li_2CO_3, respectively. We use the Tafel form in Eq. (17) rather than the Butler–Volmer form because the large kinetic overpotential during cell discharge puts the reaction in the Tafel region and considers only discharge (irreversible for O_2^- formation). It has been demonstrated that the chemical reaction in Eq. (18) is found to be first-order with to respect to both O_2^- with CO_2 reactants and is the rate determining step (RDS). Hence, the other reaction is considered as equilibrium and the formation of Li_2CO_3 can be predicted by using Eqs. (17) and (18) together.

For mechanism 2, the reduction of CO_2 in non-aqueous solvent is considerable for the Li_2CO_3 formation. The kinetic for the reaction in mechanism 2 was systematically proposed by Welford and coworkers [33] and adopted for this simulation as summarised in the follow reaction

$$r_V = k_{eff}\left(c_{CO_2}\right) \tag{19}$$

in which

$$k_{eff} = \frac{k_1}{1+K'}\exp\left[\frac{-\alpha F}{RT}\eta_m\right] \tag{20}$$

where

$$K' = \frac{k_1}{k_2}\exp\left[\frac{-\alpha F}{RT}\eta_m\right] \tag{21}$$

where k_1 and k_2 are the rate constant for the electrochemical reaction for the mechanism of the reduction of CO_2 and α is the transfer coefficient which is given the value as 0.43 [33]. However, preliminary simulated results showed that the discharge product of Li_2CO_3 mostly comes from the electrochemical in mechanism 1 rather than from the reduction CO_2 in mechanism 2.

3.2.3.3. Solvent degradation. The CO_2 generation can be created from the electrolyte degradation which is first attacked by the superoxide formation as described in Eq. (VI). Apart from this decomposition, some reports demonstrate that side reactions to form CO_2 were observed at the cathode and were attributed to

carbon decomposition during charge process [20,42]. However, only the CO_2 generated from electrolyte degradation will be considered here. Addressing this kinetic expression, because a detailed mechanism is not available, the CO_2 formation based on the overall reaction in Eq. (VI), which consider the solvent concentration as constant is:

$$j_{VI} = Fk_{VI}(c_{O_2})\left[-\exp\left(\frac{-\beta nF}{RT}\eta_m\right)\right] \quad (22)$$

where k_{1a} is the rate constant for the electrochemical reaction to form CO_2 and the others are the same as described above.

3.2.4. Rate expressions at anode

The electrochemical reaction rate for the anode includes the oxidation of lithium metal to soluble Li^+. It is described by a general Butler–Volmer equation as follow

$$j_a = i_0\left[\exp\left(\frac{(1-\beta)nF}{RT}\eta_a\right) - \exp\left(\frac{-\beta nF}{RT}\eta_a\right)\right] \quad (23)$$

where i_0 is exchange current density for anode, η_a is surface or activated overpotential for reaction at anode, and the other parameter are as described above.

The specific area, a of the electrode/electrolyte interface in Eq. (24) is decreased by the morphology and dynamic change of the porosity due to the discharge products of Li_2O_2 and Li_2CO_3 solid. These products are insoluble in several non-aqueous electrolytes and coverage the active surface area during cell operation. The variation of effective local surface area per unit volume of electrode can be commonly written by a geometric relation [43,44]

$$a = a_o\left[1 - \left(\frac{\varepsilon_s}{\varepsilon^o}\right)^p\right] \quad (24)$$

where ε_s and ε^o are the volume fraction of discharge products of Li_2O_2 and Li_2CO_3 solid, and initial electrode porosity, respectively. This empirical equation is used to describe the change in the interfacial area for electrochemical reactions that occur during discharge because of the fast passivation of Li_2O_2 and Li_2CO_3 covering a portion of the active sites for electrochemical reaction over the carbon surface [45]. The magnitude of exponent p is a geometrical factor indicating the morphology shape of the solid peroxide that covers the active area. Small values of p indicate that the flat, plate-like precipitate of Li_2O_2, conversely, large values of p reflects the needle-like solid which cover small active area. In this model, the value of 0.4 has been used.

The porosity volume change of the carbon electrode will be decreased due to the formation of insoluble solid products covering the catalyst and active particles as described in Eq. (25). Thus, the effective diffusivity for both Li^+ and all the species inside the cell is used to describe how the pores are influenced by Li_2O_2 and Li_2CO_3 formation; this can be described by the Bruggeman relationship (referred to Eqs. (6)–(9)). Because the solid distributions in the model are Li_2O_2 and Li_2CO_3, we use the properties of these solids for all of the discharge products formed

$$\frac{\partial \varepsilon}{\partial t} = \sum_{\text{solid phase } m} a j_m \frac{M_m}{nF\rho_m} \quad (25)$$

The volume fraction of the discharge solid formation can be determined from the cathode volume balance as

$$\varepsilon_s = 1 - \varepsilon - \varepsilon^o \quad (26)$$

where M_m and ρ_m are the molecular weight and the mass density of solid discharge products, respectively.

3.3. Initial conditions

To solve the governing equation for the battery cycling process, initial conditions are specified for all the species concentration inside the electrochemical cell, the porosity, the specific interfacial area, and the cell thickness. These initial values applied in the Li–air battery model are adopted from literature and summarised in Table 1. Before starting the discharge battery, the concentration for each species is assumed to uniformly distribute at all locations inside the cell system and equals to their initial concentration. Because the thickness of the porous cathode is much larger than both of APL and separator, then this area is regarded as the critical region of the computational domain affecting the cell performance.

3.4. Boundary conditions

From Fig. 1, a schematic view of the model cell consists of four boundaries and three domain regions. The constant for oxygen concentration feeding at the right side of the cathode ($x = L$) can be estimated form the oxygen solubility (S_{O_2}) and the external concentration ($c_{O_2,\,ext}$)as shown in Table 1. At the current collector or the back side of the cathode electrode ($x = L$), the current density in the solid phase is equal to the applied discharge current density, the current density in the electrolyte phase equals to zero, and the flux of each species is zero. At the cathode electrode/separator interface ($x = L_c$) the continuous boundary conditions are specified for the fluxes of all species. The current density in the solid phase in this interface becomes zero, and the current density in the electrolyte then equals to the applied discharge current density. The voltage of the cell is calculated by the difference between the electrode potential at cathode current collector and the electrolyte potential at the anode side, $V_{cell} = \phi_1(x = L) - \phi_2(x = 0)$.

The conservation equations and the boundary conditions described above were discretized using a finite element method and solved in one-dimensional battery system by commercial software package COMSOL multiphysics version 4.3. The COMSOL software is designed to solve a set of coupled differential and algebraic equations and the battery simulation model is performed on a 32 bit Windows platform with 4 GB RAM, and Intel Core 2 Duo 2.93 GHz processor. The different transport equations and the electrochemical reactions were solved as time dependent until the cell voltage reached the stop condition. The solution was considered as converged solution when the difference between two results was less than 10^{-4} (relative tolerance) for all variables.

4. Results and discussion

The one-dimensional Li–air cell model including parasitic reactions from electrolyte degradation was simulated and tested against the performance during battery cycling. As mentioned before, this model was based on previous work created by the author and could be validated by using the experimental cycle performance obtained in our labs, due to sufficient rechargeable data. A comparison of the simulated and experimental Li–air battery cycling behaviour is shown in the next section (Section 4.1). As can be seen from Fig. 3, the discharge capacity from the experimental data and simulation results were in good agreement and the model predicted the typical trend of the Li_2CO_3 accumulation on cycling resulting in electrode passivation and capacity fading.

4.1. Cycling performance

To predict the variation of the capacity retention on cycling behaviour, the variation of voltage on discharge and charge curve for 10 cycles of rechargeable Li–air battery in 1 M $LiPF_6$ dissolved in

Table 1
Parameters used in simulation.

Parameter	Value	Unit	Symbol	Ref.
Cell properties				
Thickness of APL	5×10^{-8}	m	L_A	[6]
Thickness of separator	5×10^{-5}	m	L_C	[6]
Thickness of porous positive electrode	7.5×10^{-4}	m	L	[6]
Conductivity of positive electrode	10	S m^{-1}	σ	[48]
Porosity	0.73	–	ε^o	[49]
Specific interfacial area of cathode	3.75×10^6	m^2 m^{-3}	a	Calculated
Electrical resistivity across Li_2O_2 film formation	50	Ω m^2	R_{film}	[50]
Electrolyte properties				
Electrolyte concentration	1000	mol m^{-3}	$c_{Li,0}$	[9]
Solubility factor of oxygen	0.38	–	S_{O_2}	[48]
External oxygen concentration in air at 1 atm	9.46	mol m^{-3}	$C_{O_2,ext}$	[48]
Initial oxygen concentration at $x = L$ (S_{O_2}*$c_{O_2,ext}$)	3.264	mol m^{-3}	$c_{O_2,0}$	[48]
Li^+ diffusion coefficient[a]	2.11×10^{-9}	m^2 s^{-1}	D_{Li}	[51]
Oxygen diffusion coefficient	7×10^{-10}	m^2 s^{-1}	D_{O_2}	[22]
Superoxide diffusion coefficient	9×10^{-10}	m^2 s^{-1}	$D_{O_2^-}$	[1]
Carbon dioxide diffusion coefficient	1×10^{-9}	m^2 s^{-1}	D_{CO_2}	[31]
Conductivity of Li^+ in electrolyte	1.085	S m^{-1}	κ	[52]
Transference number of Li^+[a]	0.2594	–	t_+	[53]
$\partial \ln f / (\partial \ln c_{Li})$[a]	−1.03	–	–	[53]
Kinetic parameters				
Reaction rate coefficient anodic current	1.11×10^{-15}	m s^{-1}	k_a	Assumed
Reaction rate coefficient cathodic current	3.4×10^{-17}	m^7 s^{-1} mol^{-2}	k_c	Assumed
Reaction rate coefficient for O_2^- formation	8.1×10^{-15}	m s^{-1}	k_{1a}	Assumed
Reaction rate coefficient for Li_2CO_3 formation	370	m^3 s^{-1} mol^{-2}	k_{1b}	[31]
Reaction rate constant of CO_2 reduction	1×10^{-23}	m s^{-1}	k_1	[33]
Reaction rate constant of CO_2 reduction	4.22×10^{-13}	m s^{-1}	k_2	[33]
Reaction rate constant of CO_2 formation	5.9×10^{-15}	m s^{-1}	k_{VI}	[47]
Exchange current density for anode	1	A m^{-2}	i_0	Assumed
Symmetry factor	0.5	–	β	[48]
General parameter				
Mass density of lithium peroxide (Li_2O_2)	2140	kg m^{-3}	$\rho_{Li_2O_2}$	[54]
Mass density of electrolyte solution ($LiPF_6$)	1200	kg m^{-3}	ρ_{LiPF_6}	[54]
Mass density of lithium carbonate (Li_2CO_3)	2110	kg m^{-3}	$\rho_{Li_2CO_3}$	[54]
Mass density of carbon	2260	kg m^{-3}	ρ_c	[54]
Operating temperature	300	K	T	

[a] Vary with concentration.

a non-aqueous solvent operating between 2.2 and 4.2 V vs Li/Li^+ at a rate of 0.1 mA cm^{-2} is shown in Fig. 2. This cycling model was carried out at an operating temperature of 300 K in pure 1 atm of oxygen. It can be seen from the discharge and charge cycle that the cell potential began to fall steeply at the first discharge, from a voltage of 3.1 V to a plateau at around 2.7 V, and decreased continuously to 2.2 V. The discharge potential during cycling was around 2.5–2.7 V which was the same as discharge voltage of Li–air batteries reported by previous research works for similar battery discharge in pure oxygen [16,46]. In contrast, the charge voltages increased overtime around 4.0–4.25 V depending on a number of cycles. This increase in charging overpotential could be attributed to the loss of cathode active surface due to the repeated passivation from Li_2CO_3 occurred from the electrolyte degradation during discharge. It is apparent from the figure that the reduction of capacity occurs mainly on charging, i.e. each cycle the charge capacity is lower than that during discharge step. This makes the charge/discharge efficiency less than 100% and causes the rapid capacity fading. From the data in Fig. 2, the charge potentials move to values approximately 100–200 mV higher on cycling, whereas the average discharge potentials slightly decrease. In summary, the Li–air cell model including the Li_2CO_3 formation from electrolyte degradation exhibits the cycling ability and the continuously battery capacity fading on cycling.

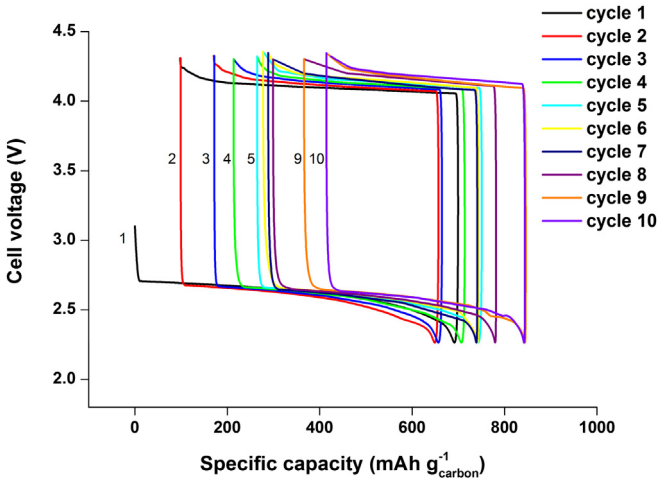

Fig. 2. Variation of voltage–capacity curve in 10 cycles on discharge and then charge between 2.2 and 4.2 V versus Li/Li^+ for a non-aqueous Li–air battery at a rate of 0.1 mA cm^{-2}. The electrolyte contains 1 M $LiPF_6$ dissolved in acetonitrile under 1 atm of oxygen at operating temperature 300 K. The cathode electrode thickness is 750 μm with porosity of 0.73.

In practice, one of the most significant properties for battery other than its initial performance is stability which can be measured by retention of discharge capacity on cycling [3,8,16,46]. Thus, for better clarity, the results obtained from the cycling behaviour of Fig. 2 are presented in more details in term of the variation of specific capacity on discharge (capacities are expressed per gram of carbon in the electrode) and retention of capacity as shown in Fig. 3. The discharge capacity on the first cycle using the parameters in Table 1 was about 700 mAh g^{-1}_{carbon}, based on the weight of carbon alone. However, on continuous discharging, the

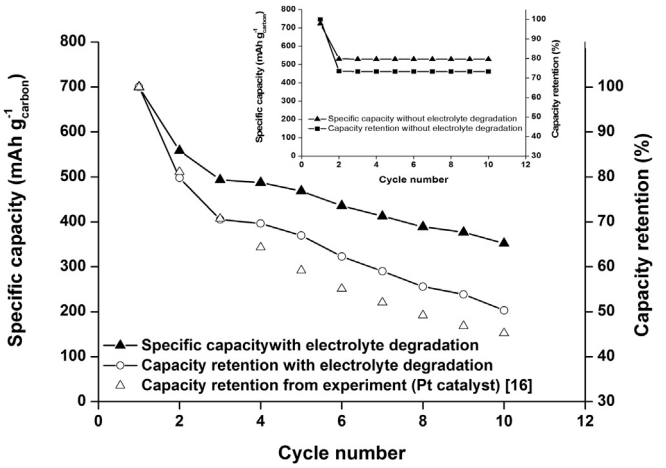

Fig. 3. The cycle performance (discharge capacity and capacity retention against cycle number) of the 10-cycle rechargeable Li–air battery in the model that includes the Li_2CO_3 formation from the electrolyte degradation. Battery was cycled at a rate 0.1 mA cm^{-2}. The capacity retention from the model and our group experiment is also plotted for comparison. The inset shows the model without the effect of electrolyte decomposition. The other parameters used in the model are the same as described in Fig. 2.

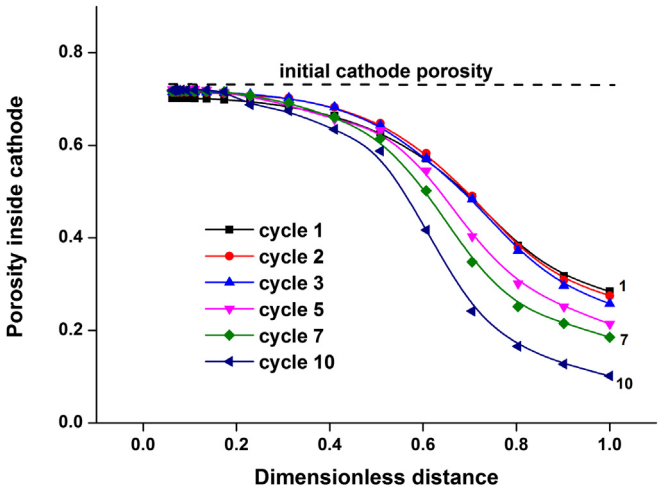

Fig. 4. Local porosity profiles inside the Li–air cell collected at the end of each discharge cycles at a rate 0.1 mA cm^{-2}. The parameters used in the model are the same as described in Fig. 2.

rechargeable Li–air battery is faced the performance deterioration on cycling. The capacity of the battery fell constantly to a low value of 468 mAh g^{-1}_{carbon} after 5 cycles which can retain the capacity back to around 67%, corresponding to a capacity retention of 13% per cycle. At the 10th cycle, the discharge capacity was even lower to 352 mAh g^{-1}_{carbon} with a capacity retention of 5% per cycle. For comparison, Fig. 3 has an inset that demonstrates the performance of a rechargeable Li–air model without any parasitic reaction form the electrolyte degradation. Without the side reaction, the Li–air battery can maintain its performance during cycling, but this is the ideal case for the Li–air battery and the researchers are still developing the batteries which remain stability on operation.

To see if the parasitic model gave the similar results with the experimental measurements [16], the battery performance data obtained in our lab were plotted and compared with the model results as also shown in Fig. 3. Because of the difference on discharge capacities acquired from the variety of Li–air cell configuration and materials, the data from the experiment could be normalised in term of the capacity retention for use as a comparison. As can be seen from Fig. 3, the experimental results from Li–air with catalyst are similar to those from the simulation model. The capacity retention of a rechargeable Li–air battery with carbon-supported Pt catalyst demonstrated a slightly lower value than the model results, with a difference of around 5% of retention. However, the catalytic battery was probably confronted performance deterioration by other factors which include degradation of carbon cathode materials as well as formation of other soluble (and insoluble) products and intermediates, which gradually decreased with the same trend as in the model results. Overall, from this study, the model results and experimental data seem to be in good agreement or at least, this model showed more reliability in predicting the cycling behaviour than that which excludes Li_2CO_3 accumulation from electrolyte degradation (inset of Fig. 3). The model is potentially a promising tool to identify the Li–air cell degradation mechanisms and forecast the cell performance for new cell designs and scale-up.

To investigate the effect of electrolyte degradation on the porous electrode, Fig. 4 compares the results for the porosity profiles inside the cathode obtained at the end of discharge in each battery cycle. The Li–air cell was cycled at a rate of 0.1 mA cm^{-2} between a discharge and charge potential of 2.2 and 4.3 V which was the same detail as presented in Fig. 2. During each cycle, the discharge products preferentially deposit near the oxygen feed side (at $x = L$ in Fig. 1) due to the slow diffusion and small solubility of O_2 preventing some of the active area of the cathode from taking part in the reaction. This behaviour is similar to that presented in our previous work [28]. On cycling, it is apparent from the graph that the available porosity of the rechargeable battery especially near the far side of electrode ($x = L$) continuously decreases at the end of each discharge cycle. The porosity in the cathode after the end of first cycle was about 0.28 cf. the initial value of 0.73. From this result, it is worth noting that the terminating discharge of Li–air battery was not the direct result of the clogging pore at the cathode surface being the limiting factor for discharge capacity, because there are still some available pores for the access of reactant species. The termination of the cell discharge process could be attributed to the rapid build-up of the discharge products of both Li_2O_2 and Li_2CO_3 covering the active sites on the carbon active surface. This cell termination from products passivation is consistent with the conclusions from both the experimental work [45] and the Li–oxygen simulation model [47]. When the cell was repeatedly operated until the end of 10th cycle, the available porosity at the

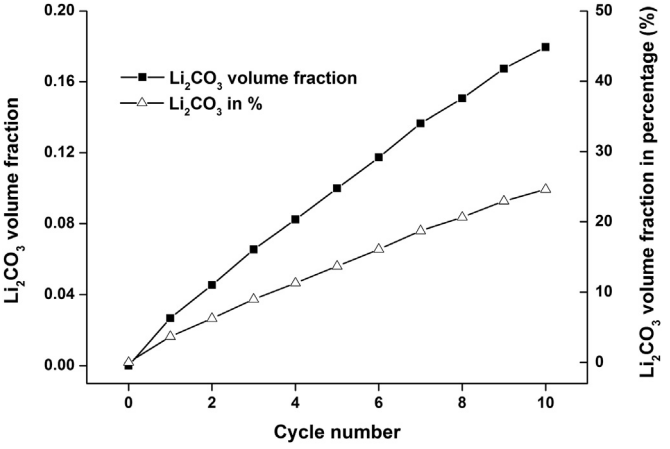

Fig. 5. Volume fraction of Li_2CO_3 formation inside the Li–air cell at the end of each discharge cycle. The Li_2CO_3 volume fraction in percentage is also plotted. The parameters used in the model are the same as described in Fig. 2.

porous electrode/current collector interface fell to only 0.1 as shown in Fig. 4. The result may be explained by the fact that the porosity of the discharge cathode is affected by the accumulation of Li_2CO_3 on cycling which is oxidised during charging (Li_2CO_3 can involve in oxidation reaction during charge process only in high charging potential >4.2 V which is not considered in this simulation study). As can be seen in Fig. 5, the volume fraction of Li_2CO_3 steadily increases and gradually deposits inside the cathode with repeated cycling of the Li–air cell, from a volume fraction percentage about 3.7% on the first cycle to 24% in the final cycle.

5. Conclusions

In this study, our previous micro–macro homogeneous model for a rechargeable Li–air battery has been developed to include the practical feature of Li_2CO_3 formation which normally occurs from electrolyte degradation during battery cycling. The modified model can successfully predict the Li–air cell cycling behaviour which starts from the first discharge to the cell potential of 2.2 V and charges until 4.2 V in 10 cycles. The cycle performance deterioration measured in term of retention of discharge capacity on cycling was predicted from the developed model which includes the effect of irreversible Li_2CO_3 discharge product. As a result, we obtain a good agreement between this cell cycling simulation and porous-electrode experiment data, thus creating a more reliable model for a rechargeable Li–air battery in non-aqueous electrolyte. Consequently, the charging voltage slightly increases in each cycle during the recharging process. This result is partly due to the repeated passivation of discharge products on the porous carbon, which lead to decrease in electrochemical active area. The termination of the cell discharge is not from pore blockage by the depositing discharge products as there are some available pores at the end of each discharge cycle. The cathode porosity decreases overtime during cycling while the volume fraction of Li_2CO_3 gradually increases in a number of cycles. The present model developed here considers only Li_2O_2 as the main discharge product and Li_2CO_3 as the byproduct coexisting during battery discharge process. Thus, the main conclusions of our modelling work are only applicable when the Li–air cell follows the formation of Li_2O_2 and Li_2CO_3 as the final discharge products.

Acknowledgements

The authors would like to thank the Ministry of Science and Technology, Royal Thai Government for funding Ukrit Sahapatsombut PhD research and to the UK EPSRC for funding under grant number EP/I022570/1.

Nomenclature

a	specific interfacial area ($m^2\ m^{-3}$)
c_i	concentration of species i (mol m^{-3})
D_i	diffusion coefficient of species i ($m^2\ s^{-1}$)
$D_{i,\mathrm{eff}}$	effective diffusion coefficient of species i ($m^2\ s^{-1}$)
E	electrode potential of cathode at any state (V)
E^0	electrode potential of cathode at standard state (V)
f	activity coefficient of $LiPF_6$ salt
F	Faraday's constant (96,485 C mol^{-1})
i_1	current density in the electrode phase (A m^{-2})
i_2	current density in the electrolyte phase (A m^{-2})
j	interfacial transfer current density of reaction m (A m^{-2})
k	reaction rate constant
L_A, L_C, L	thickness of APL, separator, and porous cathode respectively (m)
M_i	symbol for the chemical formula or molecular weight of species i (mol kg^{-1})
n	number of electrons transferred in the electrode reaction
N_i	molar flux of species i (mol $m^{-2}\ s^{-1}$)
p	surface effect factor
r_i	reaction rate term in Eq. (1) that accounts for electrochemical and chemical reactions (mol $m^{-3}\ s^{-1}$)
R	universal gas constant (8.3143 J $mol^{-1}\ K^{-1}$)
R_{film}	electrical resistivity across Li_2O_2 film formation ($\Omega\ m^2$)
s_i	stoichiometric coefficient of species i in electrode reaction
S_{O_2}	solubility factor of O_2 in non-aqueous electrolyte
t	time (s)
t_+	transference number of cation in electrolyte
T	temperature (K)
V_{cell}	cell voltage (V)
z_i	valence of charge number of species i

Greek letters

α	transfer coefficient
β	symmetry factor
ε	porosity or void volume fraction of porous cathode
ε_s	volume fraction of solid phase of porous cathode
η	surface or activated overpotential (V)
κ	conductivity of electrolyte (S m^{-1})
κ_{eff}	effective conductivity of electrolyte (S m^{-1})
ν	number of moles of ions into which a mole of electrolyte dissociates
ν_+	numbers of moles of cations produced by the dissociation of a mole of electrolyte
ρ_i	density of a solid phase of species i (kg m^{-3})
σ	conductivity of the electrode (S m^{-1})
σ_{eff}	effective conductivity of the electrode (S m^{-1})
ϕ_1	electric potential in the electrode (V)
ϕ_2	electric potential in the electrolyte (V)
$\Delta\phi_{\mathrm{film}}$	voltage drop across Li_2O_2 film formation (V)
∇	differential operator

Subscripts and superscripts

o	initial
1	electrode phase
2	electrolyte phase
a	anodic
c	cathodic
m	electrode reaction or solid species

References

[1] C.O. Laoire, S. Mukerjee, K.M. Abraham, E.J. Plichta, M.A. Hendrickson, Journal of Physical Chemistry C 113 (2009) 20127–20134.
[2] G. Girishkumar, B. McCloskey, A.C. Luntz, S. Swanson, W. Wilcke, Journal of Physical Chemistry Letters 1 (2010) 2193–2203.
[3] K.M. Abraham, Z. Jiang, Journal of the Electrochemical Society 143 (1996) 1–5.
[4] T. Kuboki, T. Okuyama, T. Ohsaki, N. Takami, Journal of Power Sources 146 (2005) 766–769.
[5] T. Ogasawara, A. Débart, M. Holzapfel, P. Novák, P.G. Bruce, Journal of the American Chemical Society 128 (2006) 1390–1393.
[6] J.G. Zhang, D. Wang, W. Xu, J. Xiao, R.E. Williford, Journal of Power Sources 195 (2010) 4332–4337.
[7] C.O. Laoire, S. Mukerjee, K.M. Abraham, E.J. Plichta, M.A. Hendrickson, Journal of Physical Chemistry C 114 (2010) 9178–9186.
[8] H. Cheng, K. Scott, Journal of Power Sources 195 (2010) 1370–1374.
[9] J. Read, Journal of the Electrochemical Society 149 (2002) A1190–A1195.
[10] J. Christensen, P. Albertus, R.S. Sanchez-Carrera, T. Lohmann, B. Kozinsky, R. Liedtke, J. Ahmed, A. Kojic, Journal of the Electrochemical Society 159 (2012) R1–R30.
[11] S.S. Zhang, D. Foster, J. Read, Journal of Power Sources 195 (2010) 1235–1240.
[12] M.W. Chase Jr., Journal of Physical and Chemical Reference Data Monographs 9 (1998) 1510.

[13] Y.C. Lu, H.A. Gasteiger, M.C. Parent, V. Chiloyan, Y. Shao-Horn, Electrochemical and Solid-State Letters 13 (2010) A69–A72.
[14] A. Debart, A.J. Paterson, J. Bao, P.G. Bruce, Angewandte Chemie – International Edition 47 (2008) 4521–4524.
[15] Z. Peng, S.A. Freunberger, L.J. Hardwick, Y. Chen, V. Giordani, F. Bardé, P. Novák, D. Graham, J.M. Tarascon, P.G. Bruce, Angewandte Chemie – International Edition 50 (2011) 6351–6355.
[16] H. Cheng, K. Scott, Applied Catalysis B: Environmental 108–109 (2011) 140–151.
[17] S.A. Freunberger, Y. Chen, N.E. Drewett, L.J. Hardwick, F. Bardé, P.G. Bruce, Angewandte Chemie – International Edition 50 (2011) 8609–8613.
[18] S.A. Freunberger, Y. Chen, Z. Peng, J.M. Griffin, L.J. Hardwick, F. Bardé, P. Novák, P.G. Bruce, Journal of the American Chemical Society 133 (2011) 8040–8047.
[19] L. Cecchetto, M. Salomon, B. Scrosati, F. Croce, Journal of Power Sources 213 (2012) 233–238.
[20] W. Xu, J. Hu, M.H. Engelhard, S.A. Towne, J.S. Hardy, J. Xiao, J. Feng, M.Y. Hu, J. Zhang, F. Ding, M.E. Gross, J.G. Zhang, Journal of Power Sources 215 (2012) 240–247.
[21] B.D. McCloskey, D.S. Bethune, R.M. Shelby, G. Girishkumar, A.C. Luntz, Journal of Physical Chemistry Letters 2 (2011) 1161–1166.
[22] J. Read, K. Mutolo, M. Ervin, W. Behl, J. Wolfenstine, A. Driedger, D. Foster, Journal of the Electrochemical Society 150 (2003) A1351–A1356.
[23] S.D. Beattie, D.M. Manolescu, S.L. Blair, Journal of the Electrochemical Society 156 (2009) A44–A47.
[24] F. Mizuno, S. Nakanishi, Y. Kotani, S. Yokoishi, I. Hideki, Electrochemistry 78 (2010) 403–405.
[25] J. Xiao, J. Hu, D. Wang, D. Hu, W. Xu, G.L. Graff, Z. Nie, J. Liu, J.G. Zhang, Journal of Power Sources 196 (2011) 5674–5678.
[26] W. Xu, V.V. Viswanathan, D. Wang, S.A. Towne, J. Xiao, Z. Nie, D. Hu, J.-G. Zhang, Journal of Power Sources 196 (2011) 3894–3899.
[27] W. Xu, K. Xu, V.V. Viswanathan, S.A. Towne, J.S. Hardy, J. Xiao, Z. Nie, D. Hu, D. Wang, J.G. Zhang, Journal of Power Sources 196 (2011) 9631–9639.
[28] U. Sahapatsombut, H. Cheng, K. Scott, Journal of Power Sources 227 (2013) 243–253.
[29] V.S. Bryantsev, M. Blanco, F. Faglioni, The Journal of Physical Chemistry A 114 (2011) 8165–8169.
[30] J.L. Roberts Jr., T.S. Calderwood, D.T. Sawyer, Journal of the American Chemical Society 106 (1984) 4667–4670.
[31] J.D. Wadhawan, P.J. Welford, E. Maisonhaute, V. Climent, N.S. Lawrence, R.G. Compton, H.B. McPeak, C.E.W. Hahn, Journal of Physical Chemistry B 105 (2001) 10659–10668.
[32] K. Tasaki, A. Goldberg, J.J. Lian, M. Walker, A. Timmons, S.J. Harris, Journal of the Electrochemical Society 156 (2009) A1019–A1027.
[33] P.J. Welford, B.A. Brookes, J.D. Wadhawan, H.B. McPeak, C.E.W. Hahn, R.G. Compton, The Journal of Physical Chemistry B 105 (2001) 5253–5261.
[34] R. Atkinson, International Journal of Chemical Kinetics 29 (1997) 99–111.
[35] H.J. Curran, P. Gaffuri, W.J. Pitz, C.K. Westbrook, Combustion and Flame 114 (1998) 149–177.
[36] A. Sinha, M.J. Thomson, Combustion and Flame 136 (2004) 548–556.
[37] M. Jitaru, D.A. Lowy, M. Toma, B.C. Toma, L. Oniciu, Journal of Applied Electrochemistry 27 (1997) 875–889.
[38] J. Newman, K.E. Thomas-Alyea, Electrochemical Systems, third ed., John Wiley & Sons, New York, 2004.
[39] J. Newman, W. Tiedemann, AIChE Journal 21 (1975) 25–41.
[40] W.A.v. Schalkwijk, B. Scrosati, Advances in Lithium-Ion Batteries, Kluwer Academic/Plenum Publishers, New York, 2002.
[41] D.A.G. Bruggeman, Annalen der Physik (Leipzig) 24 (1935) 636–679.
[42] M.M. Ottakam Thotiyl, S.A. Freunberger, Z. Peng, P.G. Bruce, Journal of the American Chemical Society 135 (2013) 494–500.
[43] R.M. LaFollette, D.N. Bennion, Journal of the Electrochemical Society 137 (1990) 3701–3707.
[44] C.Y. Wang, W.B. Gu, B.Y. Liaw, Journal of the Electrochemical Society 145 (1998) 3407–3417.
[45] X. Ren, S.S. Zhang, D.T. Tran, J. Read, Journal of Materials Chemistry 21 (2011) 10118–10125.
[46] A. Debart, J. Bao, G. Armstrong, P.G. Bruce, Journal of Power Sources 174 (2007) 1177–1182.
[47] P. Albertus, G. Girishkumar, B. McCloskey, R.S. Sánchez-Carrera, B. Kozinsky, J. Christensen, A.C. Luntz, Journal of the Electrochemical Society 158 (2011) A343–A351.
[48] P. Andrei, J.P. Zheng, M. Hendrickson, E.J. Plichta, Journal of the Electrochemical Society 157 (2010).
[49] Y.-C. Lu, D.G. Kwabi, K.P.C. Yao, J.R. Harding, J. Zhou, L. Zuin, Y. Shao-Horn, Energy & Environmental Science 4 (2011) 2999–3007.
[50] Q. Li, H.Y. Sun, Y. Takeda, N. Imanishi, J. Yang, O. Yamamoto, Journal of Power Sources 94 (2001) 201–205.
[51] S.G. Stewart, J. Newman, Journal of the Electrochemical Society 155 (2008) F13–F16.
[52] C.M. O'Laoire, Chemistry and Chemical Biology, Northeastern University, Boston, Massachusetts, 2010.
[53] A. Nyman, M. Behm, G. Lindbergh, Electrochimica Acta 53 (2008) 6356–6365.
[54] D.R. Lide, CRC Handbook of Chemistry and Physics, 87th ed., Taylor & Francis, Boca Raton, Florida, 2007.